

# In vivo MRS measurement of liver lipid levels in mice

J. R. Garbow,<sup>1,\*†,§</sup> X. Lin,\*\* N. Sakata,\*\* Z. Chen,\*\* D. Koh,\* and G. Schonfeld\*\*

Department of Chemistry,\* Washington University, St. Louis, MO 63130; and Departments of Radiology<sup>†</sup> and Internal Medicine\*\* and The Alvin J. Siteman Cancer Center,<sup>§</sup> Washington University School of Medicine, St. Louis, MO 63110

**Abstract** A magnetic resonance spectroscopy (MRS) procedure for in vivo measurement of lipid levels in mouse liver is described and validated. The method uses respiratory-gated, localized spectroscopy to collect proton spectra from voxels within the mouse liver. Bayesian probability theory analysis of these spectra allows the relative intensities of the lipid and water resonances within the liver to be accurately measured. All spectral data were corrected for measured spin-spin relaxation. A total of 48 mice were used in this study, including wild-type mice and two different transgenic mouse strains. Different groups of these mice were fed high-fat or low-fat diets or liquid diets with and without the addition of alcohol. Proton spectra were collected at baseline and, subsequently, every 4 weeks for up to 16 weeks. Immediately after the last MRS measurement, mice were killed and their livers analyzed for triglyceride level by conventional wet-chemistry methods. The excellent correlation between in vivo MRS and ex vivo wet-chemistry determinations of liver lipids validates the MRS method. These results clearly demonstrate that in vivo MRS will be an extremely valuable technique for longitudinal studies aimed at providing important insights into the genetic, environmental, and dietary factors affecting fat deposition and accumulation within the mouse liver.—Garbow, J. R., X. Lin, N. Sakata, Z. Chen, D. Koh, and G. Schonfeld. In vivo MRS measurement of liver lipid levels in mice. *J. Lipid Res.* 2004. 45: 1364–1371.

**Supplementary key words** magnetic resonance spectroscopy • triglyceride • fatty liver • cirrhosis

Alcoholic (1, 2) and nonalcoholic fatty liver (NAFL) (3–7) are highly prevalent in human populations and may develop into steatohepatitis and in some cases into cirrhosis requiring liver transplantation. Animal models of both conditions have been developed. Mouse models are particularly useful because genetic manipulations are highly developed in inbred mice. However, longitudinal studies require the killing of animals because no noninvasive method for quantifying liver fat is available. Here, we describe a noninvasive, nondestructive method for quantifying

the liver fat contents of the mouse using a NAFL mouse model. The overwhelming majority of NAFL cases are associated with obesity, dyslipidemia, hypertension, insulin-resistant type 2 diabetes mellitus, and atherosclerotic cardiovascular disease (8–12). This constellation defines the metabolic syndrome (13, 14). One naturally occurring cause of fatty liver is familial hypobetalipoproteinemia (FHBL). FHBL is defined by less than fifth percentile plasma levels of LDL-cholesterol and/or total apolipoprotein B (apoB), segregating in families as an autosomal dominant trait (15–17). The mean liver triglyceride content in apoB-impaired FHBL subjects is 3- to 5-fold greater than that of controls (18, 19).

In an attempt to understand the cellular/molecular bases of hypobetalipoproteinemia, several recombinant mice mimicking human FHBL have been produced (19–25). The resulting mice closely resemble their human counterparts with respect to the fatty liver phenotype. Thus, these mice could serve as good models of one genetic form of fatty liver for studies of the progression of fatty liver and on the effects of metabolic, hormonal, and therapeutic perturbations over time.

One current limitation of such studies is the absence of an accurate, quantifiable, noninvasive method for repeat assessments of liver fat in animals. In humans, the gold standard for quantifying liver fat is the liver biopsy, which is invasive and, at best, semiquantitative. The analogous procedure in animals is killing of the animal and direct analysis of liver fat by standard chemical methods after extraction. Obviously, direct sampling of livers for fat analysis is not ideal for longitudinal, follow-up studies in humans or animals. Noninvasive methods would be preferable in humans; these include ultrasound and computed tomography scanning with use of brightness scales (26). However, although these methods are noninvasive, they are not based on lipid chemical determinants. Furthermore, these methods have not been adapted to mice.

Proton magnetic resonance spectroscopy (MRS) is a powerful and versatile analytical technique that is specific,

Manuscript received 20 January 2004 and in revised form 14 April 2004.

Published, JLR Papers in Press, April 21, 2004.  
DOI 10.1194/jlr.D400001-JLR200

<sup>1</sup> To whom correspondence should be addressed.  
e-mail: garbow@wustl.edu

Copyright © 2004 by the American Society for Biochemistry and Molecular Biology, Inc.

This article is available online at <http://www.jlr.org>

noninvasive, and quantitative. As a consequence, MRS is well suited for in vivo, longitudinal studies of liver lipids in rodents. Proton MRS methods have been used widely to characterize triacylglycerols and other fatty acids in tissue and tissue extracts (27–30), and numerous MRS studies of liver lipids in humans have been described (18, 31–34). MRS measurements of liver fat levels in rats have been reported previously (35, 36). However, the wide variety of transgenic species available and the homology between mouse and human genomes make the mouse more appropriate for studying a variety of diseases than is the rat. The relatively small size of the mouse liver (a mouse weighs 25–35 g, ~10% the weight of a rat) presents a significant challenge in the development of appropriate MRS techniques. The purpose of this work was to adapt MRS technology to enable quantitative, in vivo measurement of liver fat in mice. We report on the development and validation of this methodology and on its preliminary application in longitudinal studies in mouse models of FHBL arising from induced truncation mutations of apoB. The results suggest that the MRI method may be more generally applicable to studies of liver fat in other mouse models of fatty liver, including fatty liver induced by alcohol.

## METHODS

### MRI and MRS

MR images and spectra of mice were collected in an Oxford Instruments (Oxford, UK) 4.7 tesla horizontal-bore magnet (40 cm bore) equipped with actively shielded, high-performance Magnex Scientific (Oxford, UK) gradient coils (10 cm inner diameter, 60 G/cm, ~100  $\mu$ s rise time). The magnet/gradients are interfaced with a Varian NMR Systems (Palo Alto, CA) INOVA console, and data were collected using a Stark Contrast (Erlanger, Germany) 2.5 cm birdcage radio frequency (RF) coil. Animals were anesthetized with isoflurane anesthetic and maintained under 1–1.5% isoflurane-oxygen (v/v) during the imaging and spectroscopy experiments. Multislice, respiratory-gated, transaxial spin-echo images were collected with a repetition time between acquisitions (TR) = 3 s and echo time (TE) = 20 ms.

Localized proton spectroscopy data were initially collected using both point resolved spectroscopy (PRESS) (37) and localization by adiabatic selective refocusing (LASER) pulse sequences (38). Both sequences use a combination of magnetic field gradients and frequency-selective  $\pi$  pulses (flip angle = 180°) to select a three-dimensional voxel of well-defined position and size, whose spectrum is then collected and analyzed. The PRESS method uses conventional, frequency-selective pulses, whereas LASER relies upon adiabatic RF pulses (39). These adiabatic pulses make the LASER sequence less sensitive to off-resonance effects (38), improving the overall stability and reproducibility of the measured liver spectra. As a result, all of the spectroscopy data reported herein were collected with LASER. To avoid phase distortion, LASER requires that adiabatic  $\pi$  pulses be inserted into the pulse sequence in pairs. Because voxel selection requires localization in each of three directions, the basic LASER sequence contains six adiabatic  $\pi$  pulses. As a consequence, the minimum TE in these sequences is ~30 ms. For the measurement of liver lipid levels in mice, we selected voxels that were 4 mm  $\times$  4 mm (in plane)  $\times$  3 mm. This voxel size, selected after considerable experimentation, is large enough that spectra of in-

dividual voxels have sufficient signal-to-noise ratios but are small enough to be reliably positioned within the mouse liver.

### Bayesian probability theory analysis

Bayesian probability theory (BPT) methods have been described for the analysis of magnetic resonance data (40–42). For spectral analysis, BPT allows modeling of the experimental data and extraction of the relevant spectral parameters. Here, we use BPT both to model the localized proton spectra of liver, allowing accurate estimation of relative lipid content, and to extract spin-spin relaxation ( $T_2$ ) values from exponentially decaying relaxation curves. Briefly, BPT is a time-domain analysis method, modeling experimental free-induction decay data as the sum of exponentially decaying sinusoids. The frequency, complex amplitudes, and decay rate constant of each signal in the spectrum are estimated, together with an uncertainty value for each of these parameters. For this work, the most important parameters were the relative amplitudes of the water and lipid signals in each spectrum. For  $T_2$  analyses, amplitudes of the water and lipid signals, as a function of TE, were estimated, and these amplitudes were then fit to an exponential decay rate constant ( $R_2 = T_2^{-1}$ ) plus a constant using BPT methods.

### Animals

All animal procedures were performed in accordance with the guidelines of Washington University's Animal Studies Committee. Results of two different studies, representing a total of 48 mice, are described. Two different strains of transgenic mice, designated apoB38.9 and apoB27.6, have recently been developed to investigate the role of apoB in fatty acid transport and fat accumulation in liver. In heterozygote apoB38.9 mice, a targeted apoB-38.9-producing mutation causes fatty livers as a result of the reduced ability of apoB-38.9 to transport triglycerides (23). Hypobetalipoproteinemic mice with a targeted apoB-27.6-specifying mutation demonstrate reduced capacity to transport and metabolize apoB-containing lipoprotein (24). Both of these strains, plus matching wild-type mice, were included in these studies. The apoB38.9 mice and controls were fed either high-fat or low-fat diets (vide infra) for 12–16 weeks, with MR spectroscopic data collected every 4 weeks. Similarly, the apoB27.6 mice and controls were fed a liquid diet with or without the addition of alcohol (vide infra). The use of wild-type and transgenic animals, combined with high-fat, low-fat, and alcohol diets, produced mice with liver lipids ranging from 2% to 35%, allowing us to test and validate the MRS method over a very wide range of values.

### Feeding protocols

All diets were purchased from TestDiet, a division of PMI (Richmond, IN). The high- and low-fat diets were both supplied in the form of dry pellets. For the low-fat diet, energy from protein, fat, and carbohydrate equaled 29.8, 7.1, and 63.1%, respectively. The corresponding values for the high-fat diet were 22.9, 41.9, and 35.2%. The liquid diet was made from a dry powder (LD105A) supplemented with maltodextrin (carbohydrate) and mixed with water. In this liquid diet, the maltodextrin supplies ~65% of the total calories. The alcohol diet was derived from this liquid diet by reducing its maltodextrin content and adding alcohol, so that the alcohol supplies ~25% of the calories in the diet. To help acclimate them, animals were fed the liquid diet, without alcohol, for 1 week before the collection of baseline MR data. For all animals, food intake was measured daily, and the mice were weighed twice per week to monitor their weight gain.

### Triglyceride analysis

Immediately after the last MRS measurement, each mouse was killed and its liver harvested and snap-frozen in liquid nitrogen.

Lipids were extracted from liver tissues as described previously (43). The dried lipid extracts were dissolved in 1% Triton X-100 in chloroform, dried under a stream of N<sub>2</sub>, and redissolved in water (44). A commercial kit was used for the specific determination of triglycerides (WAKO Chemicals USA, Inc., Richmond, VA). The hepatic triglyceride concentration was expressed as milligrams of triglycerides per gram of protein. Cellular protein content was determined using the spectrophotometric bicinchoninic acid protocol (Pierce, Rockford, IL).

## RESULTS AND DISCUSSION

Figure 1 shows *in vivo* localized proton spectra from the livers of two different mice, one having relatively low lipid content (bottom) and the other significantly higher lipid content (top). The inset on the bottom spectrum shows a  $\times 20$  expansion of the vertical scale. The spectra are dominated by the water signal at  $\sim 4.7$  parts per million (ppm). Other resonances in these spectra are attributable to liver lipid, with the bulk methylene ( $-\text{CH}_2-$ )<sub>n</sub> signal at 1.5 ppm, arising from aliphatic fatty acid chains, being the most prominent. Figure 2 (bottom) shows an expanded view of the aliphatic proton region of a typical, *in vivo* spectrum of high-fat liver. In addition to the bulk methylene signal, other lipid signals can be assigned to methyl ( $-\text{CH}_3$ ) protons (0.9 ppm) and protons from methylene groups proximate to carboxylic or olefinic carbons in the lipid (1.8–2.5 ppm). Figure 2 (top) displays the resonances found in this expanded aliphatic proton region using BPT, demonstrating BPT's ability to accurately model these data. BPT can accurately quantitate low-level signals, even in the presence of baseline distortions (40–42). As a consequence, we confidently included all of the aliphatic proton signals, and not just the methylene peak, in determining the lipid content of the liver. Similar BPT modeling was performed on all localized proton spectra, allowing correct determination of the relative intensities of

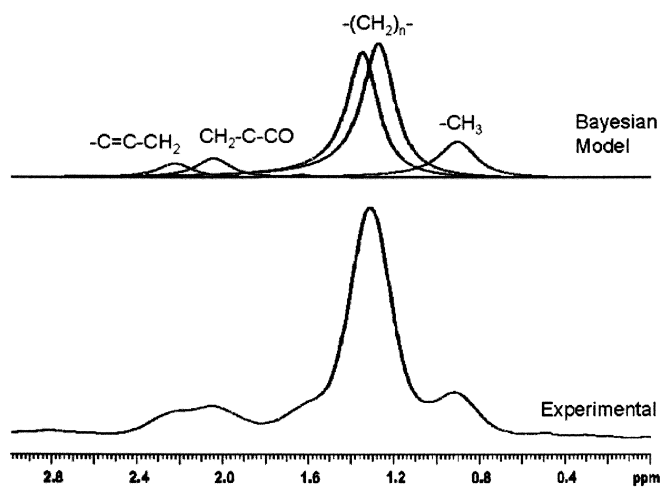


Fig. 2. Expansion of the aliphatic proton region from an *in vivo* localized proton spectrum of a high lipid level liver. Bottom: An experimental <sup>1</sup>H spectra. Top: Fourier transformation of the Bayesian probability theory (BPT) time-domain model.

lipid and water resonances. In several of the proton spectra, an additional signal attributable to olefinic (unsaturated) protons appears downfield of the water resonance, at a chemical shift of  $\sim 5.3$  ppm. In determining the liver lipid content by MRS, the amplitudes of all of these lipid signals, including the resonance at 5.3 ppm, when present, were summed and compared with the amplitude of the water resonance.

Respiratory motion can produce severe blurring of MR images, thus preventing the visualization of anatomic features at high resolution, and can also produce variations in spectral amplitude and phase in localized MR spectra (45). Therefore, accurate determination of liver lipid levels via MR spectroscopy necessitates the use of respiratory

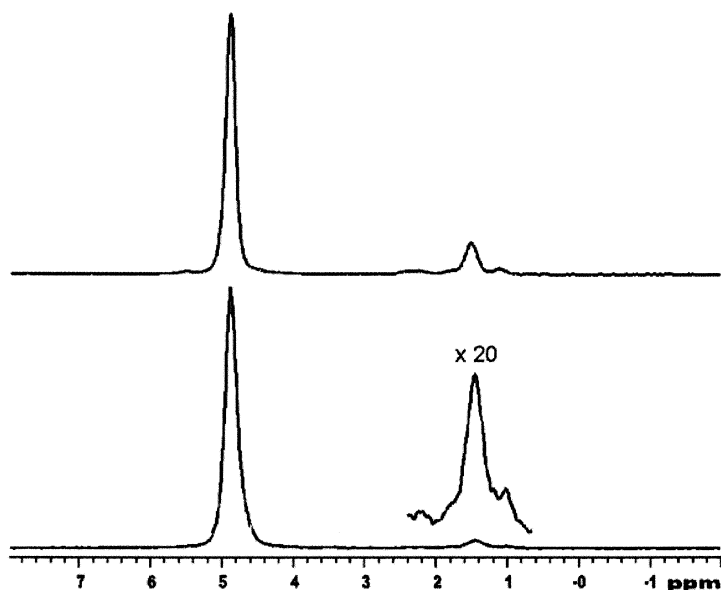
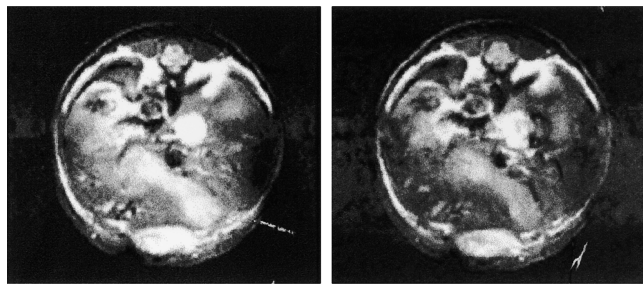


Fig. 1. Localized, *in vivo* proton MR spectra of mouse livers collected using the localization by adiabatic selective refocusing (LASER) pulse sequence with respiratory gating. The bottom spectrum shows data from a low lipid content liver, and the top spectrum shows data from a high lipid content liver. The inset on the bottom spectrum shows a  $\times 20$  expansion of the vertical scale. Experimental conditions were  $4 \times 4 \times 3$  mm<sup>3</sup> voxel, repetition time between acquisitions (TR) = 2 s, echo time (TE) = 30 ms, 16 averages. ppm, parts per million.



**Fig. 3.** Single, transaxial slices from a multislice, spin-echo MRI experiment. Left: With respiratory gating, in which data acquisition is synchronized with the animal's breathing cycle. Right: Without respiratory gating. Experiment conditions were TR = 3 s, TE = 20 ms, field of view (FOV) = 2.5 cm, slice thickness = 1 mm,  $128 \times 128$  data matrix, 4 averages.

gating techniques for the collection of both the spin-echo images required for voxel selection in the liver and the localized proton spectra from within the selected voxels. **Figure 3** shows transaxial slices of mouse liver from spin-echo images collected with and without respiratory gating. The image collected without gating (right) clearly suffers from blurring attributable to respiratory motion. This blurring, which is absent in the respiratory-gated image (left), limits significantly the accuracy with which voxels within the liver can be selected. Respiratory gating is also important for collecting localized proton spectra with peaks having consistent amplitudes and phases. **Figure 4** shows in vivo localized MR spectra from a  $4 \times 4 \times 3 \text{ mm}^3$

voxel positioned within a mouse liver collected using the LASER pulse sequence. The position of the voxel was selected from respiratory-gated spin-echo images of the liver (data not shown). The top panel shows 64 individual  $^1\text{H}$  spectra in which data collection was synchronized with respiration, and the bottom panel shows a collection of 64 spectra gathered in the absence of respiratory gating. The deleterious effects of respiratory motion on spectral amplitude and phase, seen clearly in the top panel, are nearly completely eliminated by respiratory gating.

As described above, a key to the precise determination of lipid levels is the accurate localization of the spectroscopy voxel within the liver. To improve the accuracy of the MRS measurement, reduce the dependence on specific voxel position, and ensure uniform representation of the liver, we adopted an imaging/spectroscopy protocol that involved averaging together results from several voxels within the liver. Because our MRI and MRS methods are spin-echo based, signal from flowing blood in vessels within the liver does not contribute to either images of the liver or the resulting localized spectra. In our standard MRS protocol, we first collect respiratory-gated, spin-echo multislice transaxial images of the liver. Within this set of images, we carefully select three contiguous, 1 mm thick slices that are clearly centered within the liver, as shown in **Fig. 5**. We next place a  $4 \times 4 \times 3 \text{ mm}^3$  voxel within the middle slice of these three slices, near the left-hand edge of the liver, and collect localized proton MR data (LASER; TE = 30 ms) for this voxel. The  $4 \times 4 \text{ mm}^2$  in-plane dimension of the voxel provides adequate signal-to-noise ratios in the resulting proton spectra while ensuring reliable

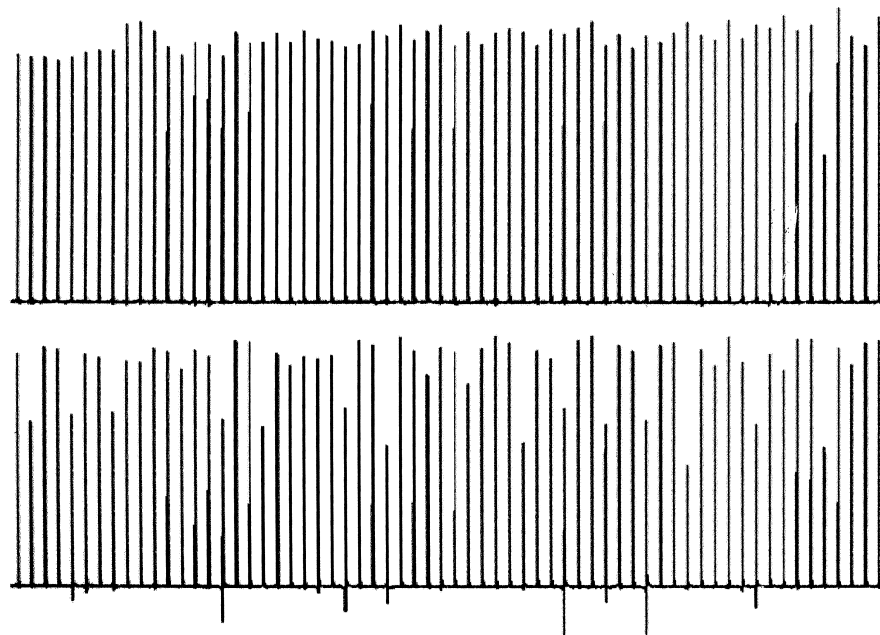


**Fig. 4.** Localized, in vivo  $^1\text{H}$  MR (LASER) spectra of mouse liver. Top: 64 individual spectra in which data collection was synchronized with respiration. Bottom: 64 individual spectra gathered in the absence of respiratory gating. The dominant signal in these spectra is the water resonance at 4.7 ppm. All data were collected from the same  $4 \times 4 \times 3 \text{ mm}^3$  voxel positioned within the liver. TR = 2 s, TE = 30 ms.



**Fig. 5.** Experimental protocol for the collection of localized, *in vivo* proton spectra of mouse liver. A set of respiratory-gated, spin-echo multislice transaxial images of the liver is collected, and within this set of images, three contiguous, 1 mm thick slices centered within the liver are selected. A  $4 \times 4 \times 3 \text{ mm}^3$  voxel is placed in the middle slice of these three slices, near the left-hand edge of the liver, and localized proton MR data (LASER; TE = 30 ms) are collected for this voxel. Because this voxel has a depth of 3 mm, it extends to include the slices shown to the left and right. The voxel is slid across the liver, in 1 mm steps, and magnetic resonance spectroscopy (MRS) data are collected at each position. Typically, data are gathered from 8 to 12 overlapped voxels for each animal. Finally, data for each voxel are analyzed separately using BPT, and the relative lipid and water percentages measured in each voxel are (separately) averaged together.

positioning within the liver. Because this voxel has a depth of 3 mm, it extends to include the slices shown to the left and right in Fig. 5. We then slide this voxel across the liver, in 1 mm steps, collecting MRS data at each position. Typically, we gather data from 8 to 12 overlapped voxels for each animal, depending on the detailed size and shape of the liver. Finally, we analyze the data for each voxel separately using BPT, averaging (separately) the relative lipid and water percentages measured in each voxel. For individual animals, the variation in measured lipid and water content across the series of overlapped voxels is typically less than 10% of the resulting average values.

The LASER proton spectra shown in Fig. 1 were collected with a TE of 30 ms. During this TE, signals attributable to both lipid and water decay as a result of the effects of transverse  $T_2$ . An accurate determination of relative lipid content must properly account for differences in  $T_2$  between the lipid and water components in liver. To address this point, for each liver lipid measurement we collected a series of five LASER spectra, with TE ranging from 30 to 50 ms, in 5 ms steps. Unlike the lipid/water composition-of-matter data, in which we measured spectra for a series of overlapping voxels, the  $T_2$  measurement for each liver was made on a single voxel chosen near the center of the organ. Intensities of lipid and water resonances were determined by BPT analysis of the individual proton spectra, and these spectral amplitudes as a function of TE were fit to single exponentials using Bayesian methods. In determining  $T_2$  (lipid) values, the amplitudes of the total lipid signal, and not those of individual spectral components, were measured and fit. Nonetheless, the measured  $T_2$  (lipid) values are essentially those of the methylene protons that dominate the lipid signal.  $T_2$  (lipid) values calculated in this manner were subsequently applied to measured total lipid signal amplitudes to account for the effects of  $T_2$  relaxation.

**Figure 6** shows representative data for water and lipid peak intensities measured in a series of variable TE LASER experiments, together with fits to the exponentially decay-

ing data. We did not discover any systematic trends in  $T_2$  values among our measurements. In particular, we found no correlation between measured  $T_2$  values and liver lipid content, no difference between  $T_2$  relaxation and strain of mouse (e.g., wild-type vs. either transgenic strain), and no correlation between lipid and water  $T_2$  values. Average values determined for a total of 165 measurements are  $T_2$  (water) = 28 ms and  $T_2$  (lipid) = 39 ms.

The decay of signal attributable to  $T_2$  relaxation is a simple exponential function of TE [i.e.,  $S(\text{TE}) = S(0) \times \exp(-\text{TE}/T_2)$ ], where  $S(\text{TE})$  is the signal amplitude measured in a LASER experiment with TE and  $S(0)$  is the amplitude of the signal at TE = 0. The  $S(0)$  values are the correct measures of lipid and water contents; consequently, amplitudes measured at TE = 30 ms were multiplied by  $\exp(30/T_2 [\text{ms}])$  to account for  $T_2$  relaxation. This relaxation correction to the MRS-determined composition-of-matter data was made on a per mouse basis, using the average lipid and water  $T_2$  values obtained for each subject.

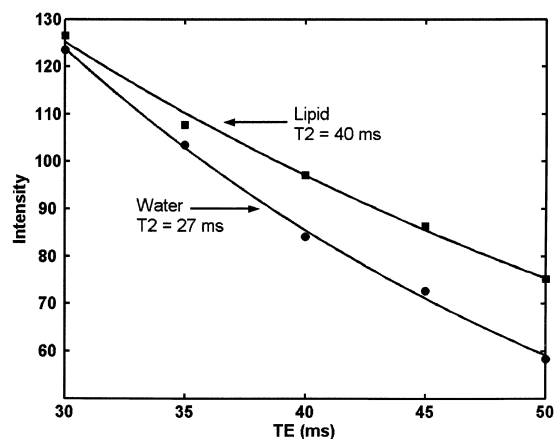


**Fig. 6.** Representative data for water and lipid peak intensities measured in a series of variable TE LASER experiments, together with fits to the exponentially decaying data. Exponential decay time constants ( $T_2$ ) are those for these specific data sets.

For each MRS measurement, we normalized the amplitude of the lipid signal (summed across all lipid resonances, averaged across all voxels) to the sum of the lipid plus water signals to obtain percentage lipid within the liver. We recognize that liver lipid is a mixture of many different fatty acids, composed of different chain lengths and degrees of unsaturation. However, all of these fatty acids are primarily composed of the same lipid building blocks, i.e., repeat units of methylene ( $-\text{CH}_2-$ ) and methine ( $=\text{CH}-$ ) groups. Thus, the ratio of total protons to molecular weight is nearly constant for all of these fatty acids, meaning that lipid proton MR signal is a proper measure of total lipid within the liver. All of the MR spectra in this work were collected with a TR of  $\sim 1.5$  s. (The exact value of TR depends on respiratory rate and thus varies slightly from animal to animal.) Variable TR experiments performed on a cohort of mice indicate that with TR = 1.5 s we overestimate the actual lipid content in liver by a factor of  $\sim 1.5$ , and we have scaled all of the results reported below accordingly. Although no comprehensive study was performed, we found no indication that  $T_1$  values in liver vary significantly or systematically with lipid content or strain of mouse (wild-type vs. either transgenic strain). This result would be expected based on the  $T_2$  relaxation data presented above. In general,  $T_2$  relaxation is more sensitive to differences in tissue character and microstructure than  $T_1$ . Thus, the absence of systematic variations in  $T_2$  values with either lipid level or mouse strain (vide supra) predicts similar behavior for  $T_1$ .

Baseline liver lipid levels for each animal were measured at the start of the study, and levels were measured again at 4 week intervals up to 8 or 12 weeks (i.e., three or four time points). Immediately after the last MRS measurement, each mouse was killed and its liver harvested

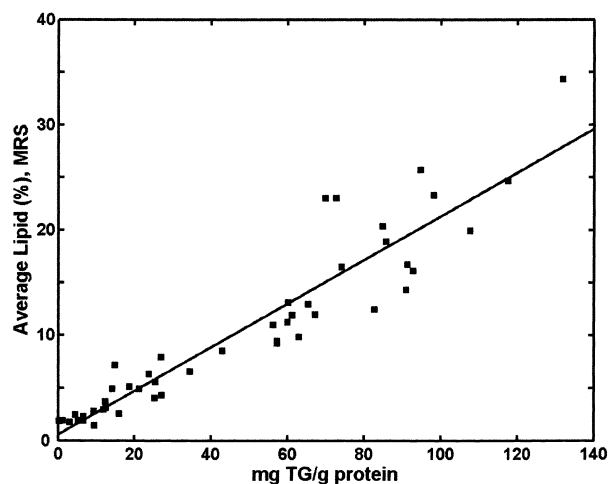



**Fig. 7.** Scatterplot showing triglyceride (TG) content (mg/g protein) plotted against MRS-determined lipid content [ $^1\text{H}$  amplitude lipid/ $(^1\text{H}$  amplitude lipid +  $^1\text{H}$  amplitude water)] for all 48 mice in this study. The correlation coefficient of the straight-line fit of these data ( $r^2 = 0.91$ ) demonstrates the excellent correlation between the in vivo and ex vivo methods and serves to validate the magnetic resonance method.

and snap-frozen in liquid nitrogen. For each liver, triglyceride levels were measured, in triplicate, using standard wet-chemical methods, as described in Methods. The wet chemistry measurement is a generally accepted method (gold standard) for determining triglyceride levels in tissue extracts. **Figure 7** is a scatterplot showing triglyceride analysis plotted against lipid determined by MRS for all 48 mice in this study. As described above, the MRS data were corrected on a per animal basis for the effects of  $T_2$ . The correlation coefficient of the straight-line fit of this data,  $r^2 = 0.91$ , demonstrates the excellent correlation between the in vivo and ex vivo methods and serves to validate the magnetic resonance method. If average  $T_2$  (water) and  $T_2$  (lipid) values are applied to all of the animals in this study, the correlation coefficient of the straight-line fit of lipid levels determined by MRS and wet-chemical methods is nearly the same ( $r^2 = 0.90$ ), consistent with the earlier observation that no systematic trends in  $T_2$  were observed in

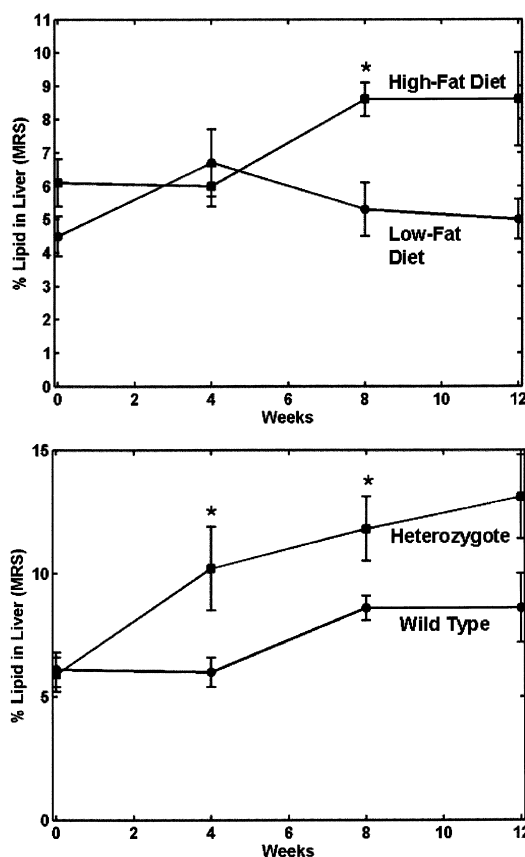


**Fig. 8.** Top: Average liver lipid level, as a function of time, for mice ( $N = 6$ ) fed high- and low-fat diets. After 12 weeks, the average lipid level in the livers of mice fed a high-fat diet is  $\sim 1.8$  times that of the animals on the low-fat diet. Bottom: Average liver lipid level, as a function of time, for transgenic (apoB27.6) and wild-type mice each fed the same high-fat diet. After 12 weeks, the liver lipid level of the apoB27.6 mice is  $\sim 1.5$  times that of the wild-type animals. Error bars represent SEM. Data were analyzed using an unpaired  $t$ -test, with statistical significance accepted at  $P < 0.05$ . Statistically different values are indicated in these plots by asterisks. The 12 week data points in the bottom plot were nearly statistically different ( $P = 0.07$ ).

these animals. The focus of this work was in correlating lipid levels measured via MRS and wet chemistry, for which a correlation coefficient alone provides the necessary measure of success. The localized MRS technique described herein could be readily extended to measure the absolute liver lipid content in mice in a manner similar to that reported in a recent study of triglyceride in human and canine liver and muscle (34).

As described in the introduction, a major motivation of this work is to develop robust *in vivo* MRS methods to permit the longitudinal study of liver lipid levels in mice. When combined with the ever-increasing variety of transgenic animal models, these techniques will provide important insights into the genetic, environmental, and dietary factors affecting fat deposition and accumulation within the liver. **Figure 8** demonstrates the promise of such measurements. In the top panel, we plot the average liver lipid level, as a function of time, for mice ( $N = 6$ ) fed high- and low-fat diets. After 12 weeks, the average lipid level in the livers of mice fed a high-fat diet is  $\sim 1.8$  times that of the animals on the low-fat diet. Similarly, the bottom panel shows the average liver lipid level, as a function of time, for transgenic (apoB27.6) and wild-type mice, each fed the same high-fat diet. After 12 weeks, the liver lipid level of the apoB27.6 mice is  $\sim 1.5$  times that of the wild-type animals. Data in both of these plots were analyzed using an unpaired *t*-test, with statistical significance accepted at  $P < 0.05$ . Another powerful application of these *in vivo* MRS measurements is the prescreening of animals before the start of a study. We have observed significant (greater than two times) variation in liver lipid levels across groups of nominally identical mice (data not shown). The ability to noninvasively measure baseline lipid levels will greatly improve the statistics of experiments aimed at studying the factors affecting liver fat deposition and accumulation, strengthening the conclusions drawn from these studies and reducing the number of animals required. 

This work was supported by National Institutes of Health Grants RO1 HL-59515 and R37 HL-42460, a National Institutes of Health/National Cancer Institute Small Animal Imaging Resource Program Grant (R24 CA-83060), and The Alan and Edith Wolf Charitable Fund.

## REFERENCES

1. Maher, J. 2002. Alcoholic steatosis and steatohepatitis. *Semin. Gastrointest. Dis.* **13**: 31–39.
2. Lieber, C. 2004. New concepts of the pathogenesis of alcoholic liver disease. *Curr. Gastroenterol. Rep.* **6**: 60–65.
3. Angulo, P. 2002. Nonalcoholic fatty liver disease. *N. Engl. J. Med.* **346**: 1221–1231.
4. Teli, M. R., O. F. James, A. D. Burt, M. K. Bennett, and C. P. Day. 1995. The natural history of nonalcoholic fatty liver: a follow-up study. *Hepatology*. **22**: 1714–1719.
5. Matteoni, C. A., Z. M. Younossi, T. Gramlich, N. Boparai, Y. C. Liu, and A. J. McCullough. 1999. Nonalcoholic fatty liver disease: a spectrum of clinical and pathological severity. *Gastroenterology*. **116**: 1413–1419.
6. Marchesini, G., E. Bugianesi, G. Forlani, F. Cerrelli, M. Lenzi, R.

- Manini, S. Natale, E. Vanni, N. Villanova, N. Melchionda, and M. Rizzetto. 2003. Nonalcoholic fatty liver, steatohepatitis, and the metabolic syndrome. *Hepatology*. **37**: 917–923.
7. Powell, E. E., W. G. Cooksley, R. Hanson, J. Searle, J. W. Halliday, and L. W. Powell. 1990. The natural history of nonalcoholic steatohepatitis: a follow-up study of forty-two patients for up to 21 years. *Hepatology*. **11**: 74–80.
8. Ikai, E., M. Ishizaki, Y. Suzuki, M. Ishida, Y. Noborizaka, and Y. Yamada. 1995. Association between hepatic steatosis, insulin resistance and hyperinsulinaemia as related to hypertension in alcohol consumers and obese people. *J. Hum. Hypertens.* **9**: 101–105.
9. Seppala-Lindroos, A., S. Vehkavaara, A. M. Hakkinen, T. Goto, J. Westerbacka, A. Sovijarvi, J. Halavaara, and H. Yki-Jarvinen. 2002. Fat accumulation in the liver is associated with defects in insulin suppression of glucose production and serum free fatty acids independent of obesity in normal men. *J. Clin. Endocrinol. Metab.* **87**: 3023–3028.
10. Zavaroni, I., S. Mazza, E. Dall'Aglio, P. Gasparini, M. Passeri, and G. M. Reaven. 1992. Prevalence of hyperinsulinaemia in patients with high blood pressure. *J. Intern. Med.* **231**: 235–240.
11. Lakka, H. M., D. E. Laaksonen, T. A. Lakka, L. K. Niskanen, E. Kumpusalo, J. Tuomilehto, and J. T. Salonen. 2002. The metabolic syndrome and total and cardiovascular disease mortality in middle-aged men. *J. Am. Med. Assoc.* **288**: 2709–2716.
12. Marchesini, G., M. Brizi, A. M. Morselli-Labate, G. Bianchi, E. Bugianesi, A. J. McCullough, G. Forlani, and N. Melchionda. 1999. Association of nonalcoholic fatty liver disease with insulin resistance. *Am. J. Med.* **107**: 450–455.
13. Reaven, G. M. 1988. Banting Lecture 1988. Role of insulin resistance in human disease. *Diabetes*. **37**: 1595–1607.
14. Reaven, G. 2002. Metabolic syndrome: pathophysiology and implications for management of cardiovascular disease. *Circulation*. **106**: 286–288.
15. Linton, M. F., R. V. Farese, Jr., and S. G. Young. 1993. Familial hypobetalipoproteinemia. *J. Lipid Res.* **34**: 521–541.
16. Schonfeld, G. 1995. The hypobetalipoproteinemias. *Annu. Rev. Nutr.* **15**: 23–34.
17. Schonfeld, G. 2003. Familial hypobetalipoproteinemia: a review. *J. Lipid Res.* **44**: 878–883.
18. Schonfeld, G., B. W. Patterson, D. A. Yablonskiy, T. S. Tanoli, M. Averna, N. Elias, P. Yue, and J. Ackerman. 2003. Fatty liver in familial hypobetalipoproteinemia: triglyceride assembly into VLDL particles is affected by the extent of hepatic steatosis. *J. Lipid Res.* **44**: 470–478.
19. Homanics, G. E., T. J. Smith, S. H. Zhang, D. Lee, S. G. Young, and N. Maeda. 1993. Targeted modification of the apolipoprotein B gene results in hypobetalipoproteinemia and developmental abnormalities in mice. *Proc. Natl. Acad. Sci. USA*. **90**: 2389–2393.
20. Srivastava, R. A., L. Toth, N. Srivastava, M. E. Hinsdale, N. Maeda, A. B. Cefalu, M. Averna, and G. Schonfeld. 1999. Regulation of the apolipoprotein B in heterozygous hypobetalipoproteinemic knock-out mice expressing truncated apoB, B81. Low production and enhanced clearance of apoB cause low levels of apoB. *Mol. Cell. Biochem.* **202**: 37–46.
21. Kim, E., C. M. Cham, M. M. Veniant, P. Ambroziak, and S. G. Young. 1998. Dual mechanisms for the low plasma levels of truncated apolipoprotein B proteins in familial hypobetalipoproteinemia. Analysis of a new mouse model with a nonsense mutation in the apoB gene. *J. Clin. Invest.* **101**: 1468–1477.
22. Kim, E., P. Ambroziak, M. M. Veniant, R. L. Hamilton, and S. G. Young. 1998. A gene-targeted mouse model for familial hypobetalipoproteinemia. Low levels of apolipoprotein B mRNA in association with a nonsense mutation in exon 26 of the apolipoprotein B gene. *J. Biol. Chem.* **273**: 33977–33984.
23. Chen, Z., R. L. Fitzgerald, M. R. Averna, and G. Schonfeld. 2000. A targeted apolipoprotein B-38.9-producing mutation causes fatty livers in mice due to the reduced ability of apolipoprotein B-38.9 to transport triglycerides. *J. Biol. Chem.* **275**: 32807–32815.
24. Chen, Z., R. L. Fitzgerald, and G. Schonfeld. 2002. Hypobetalipoproteinemic mice with a targeted apolipoprotein (apo) B-27.6-specifying mutation: *in vivo* evidence for an important role of amino acids 1254–1744 of apoB in lipid transport and metabolism of the apoB-containing lipoprotein. *J. Biol. Chem.* **277**: 14135–14145.
25. Chen, Z., R. L. Fitzgerald, G. Li, N. O. Davidson, and G. Schonfeld. 2004. Hepatic secretion of apoB-100 is impaired in hypobetalipoproteinemic mice with an apoB-38.9-specifying allele. *J. Lipid Res.* **45**: 155–163.

26. Siegelman, E., and M. Rosen. 2001. Imaging of hepatic steatosis. *Semin. Liver Dis.* **21**: 71–80.
27. Marcel, S., K. Lie, and C. Lam. 1995. <sup>1</sup>H-nuclear magnetic resonance spectroscopic studies of saturated, acetylenic and ethylenic triacylglycerols. *Chem. Phys. Lipids.* **77**: 155–171.
28. Waters, N., S. Garrod, R. Farrant, J. Haselden, S. Connor, J. Connelly, J. Lindon, E. Holmes, and J. Nicholson. 2000. High-resolution magic angle spinning <sup>1</sup>H NMR spectroscopy of intact liver and kidney: optimization of sample preparation procedures and biochemical stability of tissue during spectral acquisition. *Anal. Biochem.* **282**: 16–23.
29. Waters, N., E. Holmes, C. Waterfield, R. Farrant, and J. Nicholson. 2002. NMR and pattern recognition studies on liver extracts and intact livers from rats treated with  $\alpha$ -naphthylisothiocyanate. *Biochem. Pharmacol.* **64**: 67–77.
30. Sathasivam, N., S. Brammah, L. C. Wright, and E. J. Delikatny. 2003. Inhibition of tetraphenylphosphonium-induced NMR-visible lipid accumulation in human breast cells by chlorpromazine. *Biochim. Biophys. Acta.* **1633**: 149–160.
31. Thomsen, C., U. Becker, K. Winkler, P. Christofferson, M. Jensen, and O. Henriksen. 1994. Quantification of liver fat using magnetic resonance spectroscopy. *Magn. Reson. Imaging.* **12**: 487–495.
32. Longo, R., P. Pollesello, C. Ricci, F. Masutti, B. Kvam, L. Bercich, L. Croce, P. Grigolato, S. Paoletti, B. de Bernard, C. Tiribelli, and L. Dalla Palma. 1995. Proton MR spectroscopy in quantitative in vivo determination of fat content in human liver steatosis. *J. Magn. Reson. Imaging.* **5**: 281–285.
33. Ricci, C., R. Longo, E. Gioulis, M. Bosco, P. Pollesello, F. Masutti, L. Croce, S. Paoletti, B. de Bernard, C. Tiribelli, and L. Dalla Palma. 1997. Noninvasive in vivo quantitative assessment of fat content in human liver. *J. Hepatol.* **27**: 108–113.
34. Szczepaniak, L. S., E. E. Babcock, F. Schick, R. L. Dobbins, A. Garg, D. K. Burns, J. D. McGarry, and D. T. Stein. 1999. Measurement of intracellular triglyceride stores by H spectroscopy: validation in vivo. *Am. J. Physiol.* **276**: E977–E989.
35. Hockings, P., K. Changani, A. White, D. Reid, C. Toseland, J. Birmingham, J. Osborne, D. Templeton, and R. Buckingham. 2001. Rosiglitazone reduces liver lipid in Zucker rat. I. <sup>1</sup>H MRS study (Abstract). *Proc. Int. Soc. Magn. Reson. Med.* **9**: 1039.
36. Hockings, P. D., K. K. Changani, N. Saeed, D. G. Reid, J. Birmingham, P. O'Brien, J. Osborne, C. N. Toseland, and R. E. Buckingham. 2003. Rapid reversal of hepatic steatosis, and reduction of muscle triglyceride, by rosiglitazone: MRI/S studies in Zucker fatty rats. *Diabetes Obes. Metab.* **5**: 234–243.
37. Bottomley, P. A. 1987. Spatial localization in NMR spectroscopy in vivo. *Ann. N. Y. Acad. Sci.* **508**: 333–348.
38. Garwood, M., and L. DelaBarre. 2001. The return of the frequency sweep: designing adiabatic pulses for contemporary NMR. *J. Magn. Reson.* **153**: 155–177.
39. Tannus, A., and M. Garwood. 1997. Adiabatic pulses. *NMR Biomed.* **10**: 423–434.
40. Neil, J., and G. Bretthorst. 1993. On the use of Bayesian probability theory for analysis of exponential decay data: an example taken from intravoxel incoherent motion experiments. *Magn. Reson. Med.* **29**: 642–647.
41. Kotyk, J. J., N. G. Hoffman, W. C. Hutton, G. L. Bretthorst, and J. J. H. Ackerman. 1992. Comparison of Fourier and Bayesian analysis of NMR signals. I. Well-separated resonances (the single-frequency case). *J. Magn. Reson.* **98**: 483–500.
42. Kotyk, J. J., N. G. Hoffman, W. C. Hutton, G. L. Bretthorst, and J. J. H. Ackerman. 1995. Comparison of Fourier and Bayesian analysis of signals. II. Examination of truncated free induction decay NMR data. *J. Magn. Reson. Ser. A.* **116**: 1–9.
43. Bligh, E. G., and W. J. Dyer. 1959. A rapid method of total lipid extraction and purification. *Can. J. Biochem. Physiol.* **37**: 911–917.
44. Carr, T. P., C. J. Anderson, and L. L. Rudel. 1993. Enzymatic determination of triglyceride, free cholesterol, and total cholesterol in tissue lipid extracts. *Clin. Biochem.* **26**: 39–42.
45. Garbow, J., J. Dugas, S.-K. Song, and M. Conradi. 2004. A simple, robust hardware device for passive or active respiratory gating in MRI and MRS experiments. *Concepts in Magn. Reson., Part B: Magn. Reson. Engin.* **21B**: 40–48.